



ZnO@ porous graphite nanocomposite from waste for superior photocatalytic activity

Hanan H. Mohamed^{1,2} · Amerah A. Alsanea^{1,2} · Nuhad A. Alomair^{1,2} · Sultan Akhtar³ · Detlef W. Bahnemann^{4,5}

Received: 8 November 2018 / Accepted: 22 February 2019 / Published online: 6 March 2019
© Springer-Verlag GmbH Germany, part of Springer Nature 2019

Abstract

In this work, a new type of advanced 3D mesoporous carbon nanocomposites derived from Zn dust/PET bottle mixed waste with a high surface area is created. Interestingly, simultaneous transformation of Zn metal into ZnO nanoparticles and PET bottle waste to porous carbon materials occurred upon thermal treatment at 700 °C. The effect of the amount of Zn metal on the prepared materials has been studied. The carbon material-based waste presented very large surface area (up to 684.5 m²/g) with pore size distribution (18.47–16.88 nm). The SEM and TEM analysis revealed that the produced carbon materials have 3D porous dense layers with a gradient pore structure. The created waste-based nanocomposite exhibited an enhanced photocatalytic performance for the degradation of organic dyes (methylene blue and malachite green). It is believed that the presented work not only provides a sustainable approach to the creation of new nanocomposites of ZnO-mesoporous carbon materials for the application in photocatalysis but also introduces a new way of upcycling of mixed waste materials.

Keywords PET/Zn mixed waste · Simultaneous upcycling · ZnO/graphite nanocomposite · Photocatalysis

Introduction

Upcycling wastes convert them to be finally value-added products as well as reduce the waste disposal problems. Upcycling is very important upon considering the recent increasing use of

plastic products around the world. The preparation of valuable material from plastic waste is significant both from economic and environmental points of view. Plastic production has increased markedly over the last decades, thus, leading to high levels of their disposal and generating several environmental problems. Recently, extensive researches have been made to upcycle plastic wastes into high value-added carbon nanomaterials (Chen et al. 2015; Tang et al. 2005; Lerici et al. 2015; Sharma et al. 2014; Mishra et al. 2012). Since plastic wastes consist majorly of carbon, they can be converted into carbon-based value-added products such as light hydrocarbons (Lovett et al. 1997; Buekens and Huang 1998; Yang and Lin 2009; Jan et al. 2013), activated carbon (Esfandiari et al. 2012), fullerenes (Howard et al. 1991; Howard et al. 1994; Richter et al. 1997), carbon nanotubes (Zhuo and Levendis 2014; Dai 2002; Popov 2004; De Volder et al. 2013; Dervishi et al. 2009), and graphite and graphene (Geim and Novoselov 2007; Ruan et al. 2011; Akhavan et al. 2014).

Amongst current technologies to upcycle plastic wastes, the energy recovery technologies such as thermal and catalytic pyrolysis have attracted considerable attention (Miskolczi et al. 2009; Anene et al. 2018). Recently, automobile waste car bumper has been successfully transformed into novel carbon nanomaterials using catalytic pyrolysis process in the presence of TiO₂ as catalyst (Mohamed and Alsanea 2018).

Responsible editor: Suresh Pillai

✉ Hanan H. Mohamed
hhbesisa@iau.edu.sa

Detlef W. Bahnemann
detlef.bahnemann@spbu.ru; bahnemann@iftc.uni-hannover.de

¹ Department of Chemistry, Science College, Imam Abdulrahman Bin Faisal University, P. O. Box 1982, Dammam 31441, Kingdom of Saudi Arabia

² Basic and Applied Scientific Research Center, Imam Abdulrahman Bin Faisal University, P.O. Box 1982, Dammam 31441, Saudi Arabia

³ Electron Microscopy Unit, Institute for Research and Medical Consultations, Imam Abdulrahman Bin Faisal University, P.O. Box 1982, Dammam 31441, Saudi Arabia

⁴ Laboratory “Photoactive Nanocomposite Materials”, Saint-Petersburg State University Peterhof, Saint-Petersburg, Russia 198504

⁵ Institut fuer Technische Chemie, Gottfried Wilhelm Leibniz Universitaet Hannover, Hannover, Germany

Metals are important materials that linked to industrial development and improved living standards. Metals can be used in several industrial purposes such as mining, construction, and manufacture of automobiles, airplanes, ships, and railways. They can also be used to manufacture domestic items such as cutlery, crockery, and even in the packaging. Metal wastes are discharged into the environment in the forms of wastewater, spent solution, and solid waste (Leung et al. 2008). Disposal of metal wastes into the environment can cause many serious problems to the human health and the leaving organisms (Morf et al. 2013; Zhou and Qiu 2010). Amongst metal waste, zinc is listed by the Environmental Protection Agency (USA) as one of the 129 priority pollutants (Chen and Tang 2007). In humans, prolonged excessive exposure to zinc can lead to deficiencies in iron and copper, nausea, and abdominal pain (Chen and Tang 2007). Accordingly, efficient methods are required to upcycle such hazardous metal waste into useful materials. Amongst the available methods for metal recovery are hydrometallurgical method (Jadhav and Hocheng 2015), liquid–liquid extraction (Vander Hoogerstraete et al. 2013), ion exchange (Gupta et al. 1987), and electrochemical separations (Irwin et al. 1997). Since zinc oxide nanoparticles have wide applications in cell batteries (Linden 1995), in antibacterial activity (Shinde et al. 2014; Dědková et al. 2015), and in photocatalysis (Kim et al. 1997; Schmucker 1893; Zhou et al. 2014), converting Zn metal waste to useful ZnO is a great benefit.

A lot of work has been done on the recovery of metallic zinc from galvanizing plant wastes by the production of high-purity ZnO by oxidizing zinc vapor in an oxygen atmosphere (Dvorak and Jandova 2005). The galvanizing plant waste (zinc dross) was mixed with a reducing agent (e.g., coke, activated carbon) and heated to vaporize zinc.

Upcycling separate waste such as converting plastic wastes into high-value-added carbon nanomaterials or converting metal wastes into useful metal oxide has attracted much attention; however, upcycling metal/plastic mixed waste has not yet been extensively studied. Plastic and metal waste can exist together in several manufactures such as electronic waste, medical waste, batteries, accumulators, and end-of-life vehicles. Therefore, upcycling plastic/metal mixed waste is considered to be a mature field of interest owing to its perilous impact on human life and environment. Thus, simultaneous upcycling of plastic and metal wastes is urgent.

2D sp^2 carbon nanosheet composite materials were found to be interesting materials due to their unique properties such as optical, electrical (Ding et al. 2017), and mechanical properties; therefore, there have been applied to the field of electrochemistry such as lithium-ion battery or supercapacitor (Ding et al. 2016; Memon et al. 2016), photocatalysis (Gottardi et al. 2014; Zhao et al. 2017; Mohamed and Mohamed 2018), and biological activity (Muthirulan, et al. 2013). However, the Van der Waals and π – π interaction in

the graphite sheets causing their agglomeration and limiting their practical usages. 3D porous graphite has a network structure with high surface area and high conductivity (To et al. 2015). Nanocomposites based on carbon–allotrops have a broad range of environmental applications including sorbents, membranes, filters, antimicrobial agents, environmental sensors, renewable energy technologies, and pollution prevention strategies (Mauter and Elimelech 2008; Nasir et al. 2018; Mohamed 2018; Mohamed et al. 2018). Amongst carbon-based nanomaterials, graphene oxide-based nanocomposite materials have attained considerable attention. Several synthesis methods of GO have been reported previously such as oxidation of graphite flakes, epitaxial growth by chemical vapor deposition, arc discharge of graphite, in situ electron beam irradiation, epitaxial growth on SiC, thermal fusion, laser reduction of polymers sheets, and unzipping of carbon nanotubes (Singh, et al. 2016; Xu et al. 2017).

Herein, simultaneous upcycling of plastic waste and metal waste into metal oxide/porous carbon nanocomposites has been achieved. Polyethylene tetrathalate (PET) bottle waste which is a considerable part of the total plastic waste in the environment is utilized as model plastic waste and Zn dust is utilized as a model metal waste. A facile thermal method has been used to upcycle Zn/PET bottle mixed waste into nanocomposites of ZnO nanoparticles and mesoporous graphite. The crystal structure, morphology, and surface area of produced materials were investigated using different techniques. Furthermore, the innovative Zn/PET bottle waste-derived mesoporous ZnO/graphite nanocomposites is utilized as photocatalysts. The results reveal that the created waste-based nanocomposite exhibited an enhanced photocatalytic performance for the mineralization of organic dyes. This work has wide potential applications owing to creating active materials to achieve environmental remediation utilizing waste materials and minimal cost technique to achieve one of the sustainable development targets.

Experimental method

Transformation of Zn dust/PET bottle mixed waste to porous ZnO/graphite nanocomposites

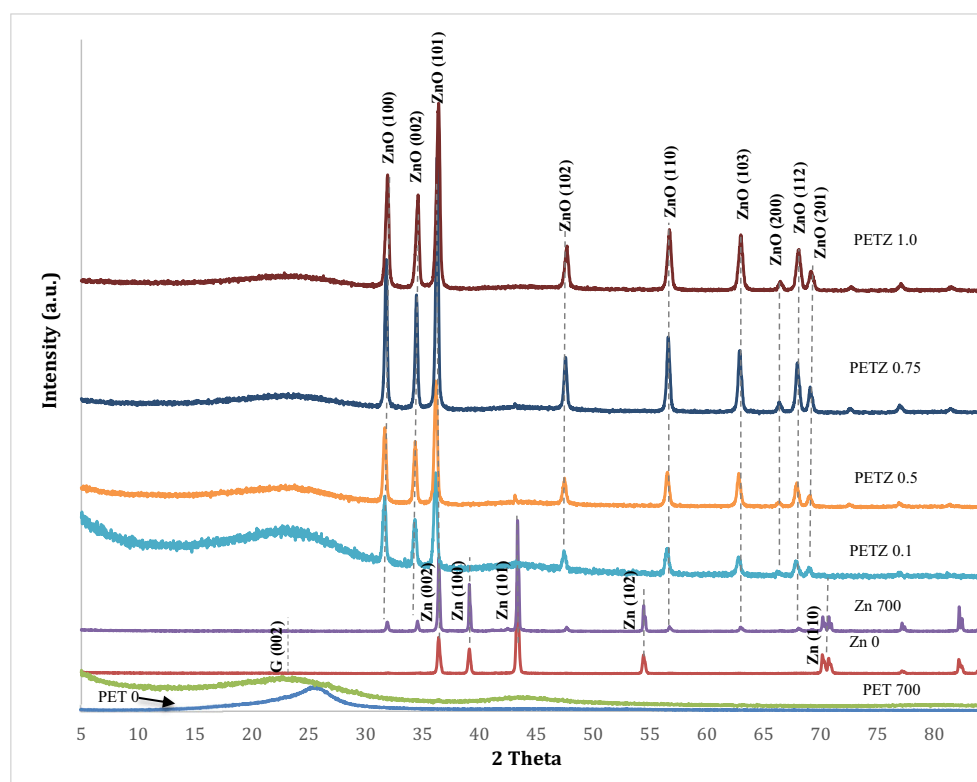
The PET bottle waste has converted to nanocomposite materials by thermal decomposition method in the presence of Zn metal. In a typical method, the plastic water bottles were divided into about 1-cm² pieces and then cleaned with pure water and dried in an open area. A specific amount of the bottle pieces was then mixed with the desired amount of zinc dust (0.1, 0.5, 0.75, 1 g) in a stainless steel vessel and then placed into muffle furnace at 700 °C. After 1 h, shiny black

powders have been obtained. For comparison, the plastic bottle pieces were thermally degraded in the absence of zinc dust and the zinc dust was thermally treated in the absence of the bottle waste under the same conditions. The samples symbolized as PET 0, PET 700, Zn 700, PETZ 0.1, PETZ 0.5, PETZ 0.75, and PETZ 1.0 respectively for the raw plastic bottles before heat treatment, the bottles after heat treatment in the absence of Zn dust, the Zn dust after heat treatment in the absence of bottle waste, and the bottles after heat treatment in the presence of Zn dust of different contents of 0.1 g, 0.5 g, 0.75 g, and 1 g, respectively.

Materials characterization

The crystal structure of the prepared materials has been determined by XRD measurements using XRD-700, Maxima. The size and morphology of the materials were obtained by SEM (FEI, INSPECT S50) and TEM measurements (FEI, Morgagni 268, Czech Republic at 80 kV). The surface area and porosity were investigated from BET measurements (Quantachrome NOVA 1200e analyzer). The thermal stability of the materials was obtained from DTA-TGA measurements (DTG-60H), and the optical properties were evaluated using Raman and UV-vis diffuse reflectance measurements. To verify the XRD data and evaluate the crystalline nature of the synthesized products locally, the electron diffraction patterns in the TEM were also captured.

Fig. 1 XRD patterns of raw plastic bottles (PET 0), raw zinc dust (Zn 0), zinc dust after pyrolysis at 700 °C (Zn 700), plastic bottles after pyrolysis at 700 °C in inert atmosphere in the absence of Zn dust (PET 700), and plastic bottles after pyrolysis at 700 °C in inert atmosphere in the presence of Zn dust of different contents (PETZ 0.1, PETZ 0.5, PETZ 0.75, and PETZ 1.0)



Photocatalytic performance

The photocatalytic performance of the waste-based materials has been determined by measuring the degradation of organic dye methylene blue (MB) and malachite green (MG) as model water pollutants. All the photocatalytic experiments were carried out using a column glass reactor with a UV lamp (365 nm). In a typical photocatalytic experiment, an optimum amount (1 g/l) of the prepared sample (PET 700, PETZ 0.1, PETZ 0.5, PET 0.75, and PET 1.0) was homogeneously dispersed in 100 ml of distilled water followed by adding of 20 mg/l of aqueous dye solutions (MB or MG) at pH 6.7. The irradiation was performed under air bubbling, and the concentration of the dyes (MB, MG) has been followed by measuring their UV-vis absorbance with a maximum at 665 nm for MB and at 635 nm for MG during illumination.

Results and discussion

Materials characterization

Figure 1 shows the XRD patterns of all samples (PET 0, PET 700, PETZ 0.1, PETZ 0.5, PETZ 0.75, PETZ 1.0, Zn 0, and Zn 700). The XRD pattern of the raw PET bottle shows the typical peak of polyethylene terephthalate at 25.4° (Murthy et al. 1991; Mauter and Elimelech 2008; Memon et al. 2016). The XRD pattern of the plastic bottle after thermal

treatment in the absence of Zn dust shows an intense peak at 23.56° which can be indexed to the $\{002\}$ peak of the graphitic structure of carbon and broad peak at 43° (Mhamane et al. 2011). The XRD pattern of zinc dust before thermal treatment shows intense peaks at 36.42° , 39.14° , 43.34° , and 54.42° , which are corresponded to the lattice planes of the hexagonal Zn crystal (JCPDS card no. 65-3358). The XRD patterns of plastic bottle after thermal treatment in the presence of different amounts of Zn dust (i.e., PETZ0.1, PETZ.5, PETZ0.75, and PETZ1) show the characteristic diffraction peaks at 31.8° , 34.4° , 36.3° , 47.5° , 56.6° , 62.9° , 66.6° , 68.1° , and 69.2° , respectively, which are characteristic to the ZnO wurtzite structure (JPCDS 36-1451) in addition to characteristic graphite peak at 23.56° with the disappearance of the peaks of Zn metal. The results reveal the complete transformation of Zn particles into ZnO nanoparticles upon thermal treatment in the presence of a plastic bottle. For comparison, the XRD pattern of (Zn 700) obtained after thermal treatment of Zn dust at 700°C in the absence of plastic bottles is measured. The result shows the characteristic diffraction peaks of the hexagonal Zn crystal in addition to weak peaks at 31.8° , 34.4° , 47.5° , 56.6° , and 62.9° of the wurtzite structure of ZnO indicating an incomplete transformation of Zn to ZnO in the absence PET bottle. Thus, a mutual transformation of plastic bottle into graphite and transformation of Zn into ZnO has occurred upon thermal treatment at 700°C .

Figure 2 shows the Raman spectra of PET 0, PET 700, PETZ 0.1, PETZ 0.5, PETZ 0.75, and PETZ 1.0. The Raman spectrum of raw plastic bottles shows the typical Raman spectrum of polyethylene tetra phthalate (PET) with two strong characteristic bands at 1725 cm^{-1} and 1613 cm^{-1} that correspond to the C=O stretching vibration (Socrates

2001; Lin-Vien et al. 1991), the band at 1290 cm^{-1} identifies the CH_2 wagging vibration and the asymmetric C–O–C stretching, the band at 858 cm^{-1} corresponds to the ester bending mode (Ajji et al. 1995; Paquin et al. 2007), and the band at 631 cm^{-1} characteristic for aromatic esters and the weak band at 1416 cm^{-1} attributed to the aromatic ring C=C stretching vibration and $-\text{OCH}_2-$ wagging vibration (Lin-Vien et al. 1991). Successful transformation of waste plastic bottle into porous graphite was further verified by Raman spectra. The Raman spectrum of the plastic bottle after heating in the absence of Zn dust (PET700) shows the characteristic D band at 1354 cm^{-1} and G band at 1580 cm^{-1} characteristic of graphitic carbon. The Raman spectra of PETZ 0.1, PETZ 0.5, PETZ 0.75, and PETZ 1.0 show the characteristic D and G band of graphitic carbon. In addition, the peaks at 437 cm^{-1} , 339 cm^{-1} , and 588 cm^{-1} , which are characteristic of ZnO, appeared for PETZ 1.0. For the samples PETZ 0.1, PETZ 0.5, and PETZ 0.75, the ZnO peaks are not predominant which may be owing to the smaller percent of ZnO in these samples.

Figure 3 shows the SEM images of PETZ 0.1, PETZ 0.5, PETZ 0.75, and PETZ 1.0. SEM images (Fig. 3a–d) show the dense layers of carbon materials with an accumulation of ZnO particles. Some carbon material exhibits very thin appearance denoted here as carbon nano-sheets (CNS). Back-scattered electron (BSE) imaging, sensitive to the atomic number, was

Fig. 2 Raman spectra of raw plastic bottles (PET 0), plastic bottles after pyrolysis at 700°C in inert atmosphere in the absence of Zn dust (PET 700), plastic bottles after pyrolysis at 700°C in inert atmosphere in the presence of Zn dust of different contents (PETZ 0.1, PETZ 0.5, PETZ 0.75, and PETZ 1.0)

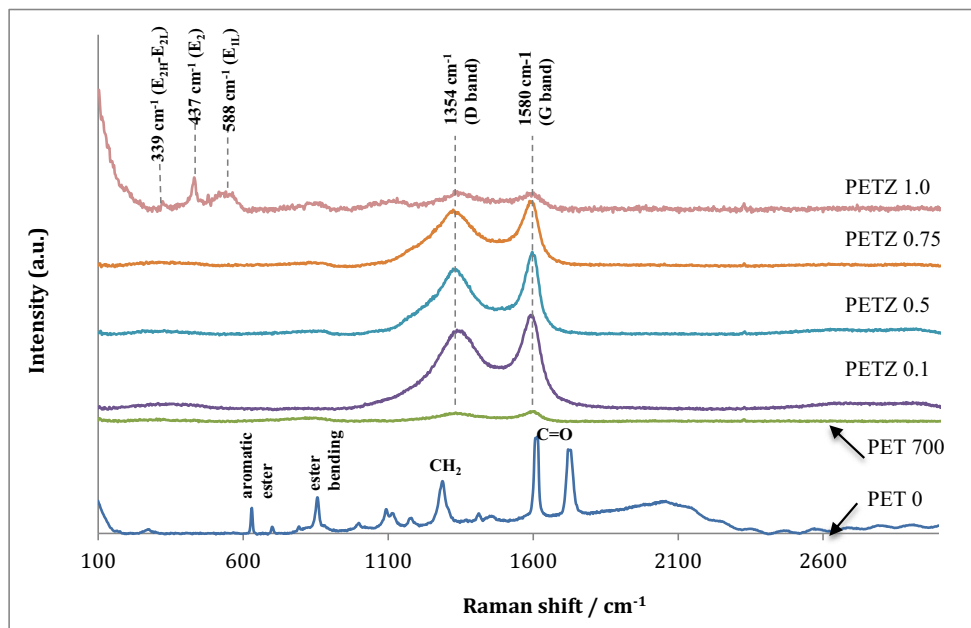


Fig. 3 SEM images ($\times 20,000$ magnification) of plastic bottles after pyrolysis at 700°C in inert atmosphere in the presence of Zn dust of different contents. PETZ 0.1 (a, a1), PETZ 0.5 (b, b1), PETZ 0.75 (c, c1), and PETZ 1.0 (d, d1). (a–d) Secondary electron (SE) and (a1–d1) are the back-scattered electron (BSE) images of the transformed products. The thin layer of carbon sheets is highlighted by white arrows and ZnO particles by white arrowheads

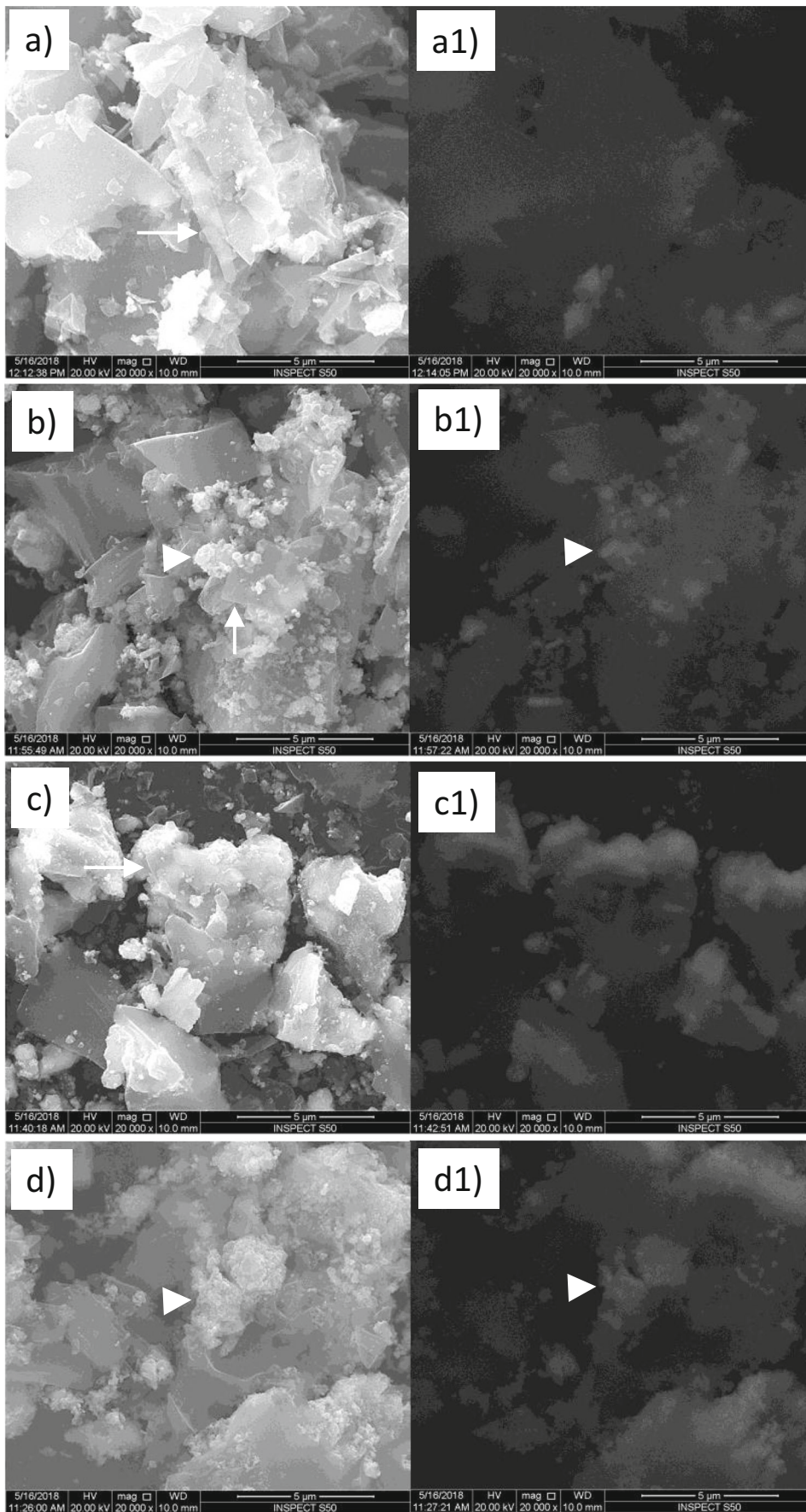
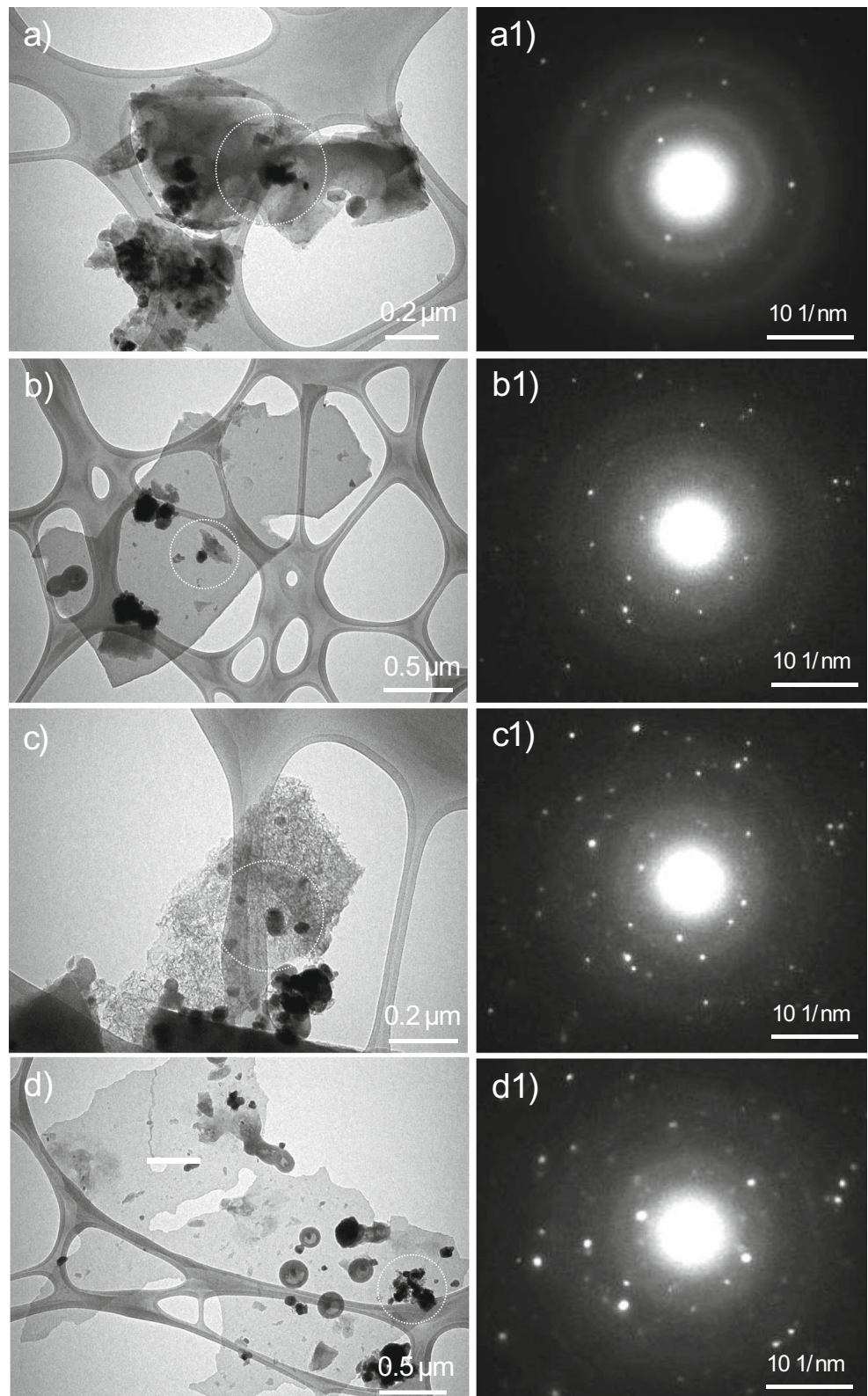


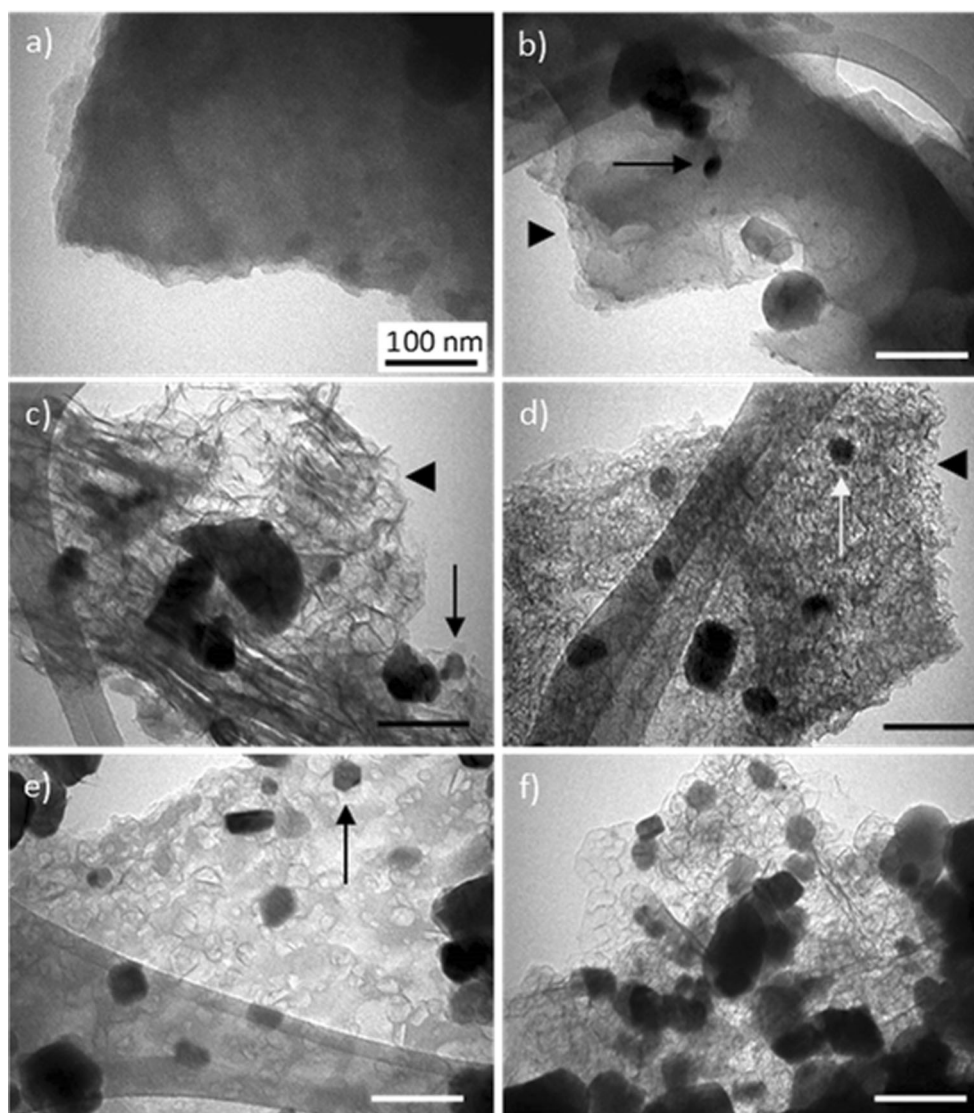
Fig. 4 TEM overview micrographs along with selected area electron diffraction (SAED) patterns of plastic bottles after pyrolysis at 700 °C in inert atmosphere in the presence of Zn dust of different content. PETZ 0.1 (a), PETZ 0.5 (b), PETZ 0.75 (c), and PETZ 1.0 (d). The area (400–500 nm) from where the electron diffraction pattern was taken in each case is indicated by a dotted white circle



also performed in order to identify the existence and distribution of ZnO particle within the CNS. The results of BSE micrographs have shown that the same area like SE images is

represented by Fig. 3a1–d1. The BSE micrographs show the existence of ZnO particles, as Zn ($Z = 30$) scattered more electrons than carbon ($Z = 6$) due to having a higher atomic

Fig. 5 (a) TEM images of plastic bottles after pyrolysis at 700 °C in inert atmosphere in the absence of Zn dust (PET 700) and (b–f) in the presence of Zn dust of different contents: (b) PETZ 0.1, (c) PETZ 0.5, (d) PETZ 0.75, and (e, f) PETZ 1.0. Nano-sheets are marked by arrowheads and ZnO particles with arrows. All scale bars correspond to 100 nm



number and appeared brighter in the carbon background. BSE electronic micrographs revealed the distribution of ZnO particles in carbon sheets. The ZnO particles were appeared either as individuals or group of several particles decorated on carbon sheets. Some sheets are highlighted by white arrows and ZnO particles by white arrowheads in each case. Figure 4 shows the TEM micrographs of plastic transformed material at low magnification, where carbon sheets along with ZnO particles can be seen. The spots of electron diffraction patterns (insets) demonstrate the crystalline nature of the prepared products, confirming that the XRD data shown in Fig. 1. Figure 5(a–f) shows the TEM images of the plastic bottle after pyrolysis in the absence of Zn dust or the presence of various content of Zn dust (PET 700, PETZ 0.1, PETZ 0.5, PETZ 0.75, PETZ 1.0). The TEM images show that the carbon materials have 3D porous layers with gradient pore structures. The prepared CNS sheets were much thinner than the carbon support used with TEM grid. The produced CNS in PET 700

were found to be much more thicker with less porosity than CNS produced from pyrolysis of PET in the presence Zn metal (PETZ 0.1). These results have been supported by the results from BET surface area analysis (Table 1). These results can explain the role of Zn metal in modifying the structure of

Table 1 N₂ adsorption–desorption characteristics of PET 700, PETZ 0.1, PETZ 0.5, PETZ 0.75, and PETZ 1.0

Sample	S_{BET} (m ² g ⁻¹)	Pore volume (cm ³ g ⁻¹)	Average pore size (nm)
PET 700	589.5	0.165	18.47
Zn 700	48.2	0.035	12.32
PETZ 0.1	684.5	0.196	18.47
PETZ 0.5	502.7	0.160	18.47
PETZ 0.75	462.0	0.138	18.47
PETZ 1.0	398.5	0.137	16.88

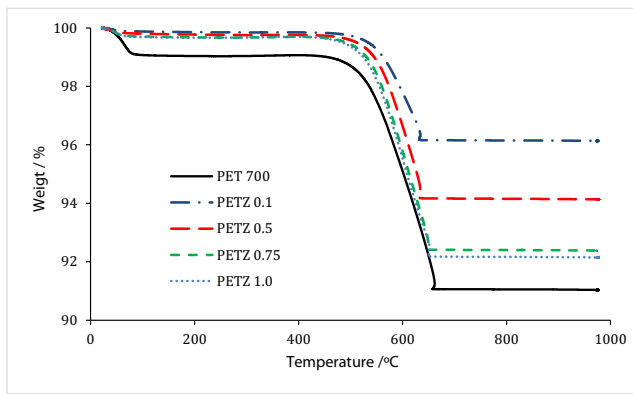


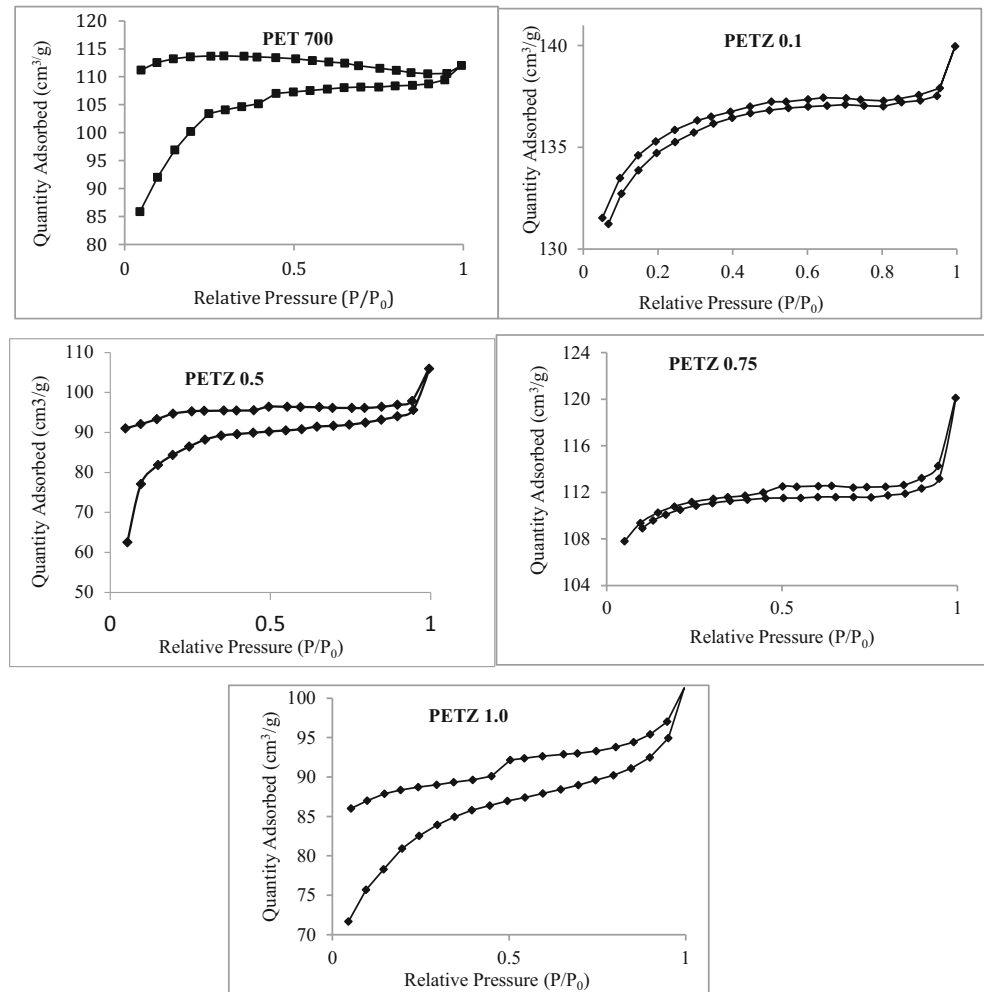
Fig. 6 TGA of plastic bottles after pyrolysis at 700 °C in inert atmosphere in the absence of Zn dust (PET 700) and in the presence of Zn dust of different contents (PETZ 0.1, PETZ 0.5, PETZ 0.75, and PETZ 1.0)

less than 50 nm. No obvious change in the morphology or porosity of the nanocomposites has been observed from the TEM measurements. As expected, the number of ZnO particles was increased with the increasing concentration of Zn metal in the synthesis. TEM observation revealed the successful transformation of plastic waste material/Zn metal into porous carbon sheets and crystalline spherical ZnO particles.

Figure 6 displays the TGA curves for PET 700, PETZ 0.1, PETZ 0.5, PETZ 0.75, and PETZ 1.0. It is shown for all samples that mass loss is observed at 150 °C which is due to the loss of hydroxyl, epoxy functional groups, and water molecules. Another mass loss at 450 °C and 650 °C involved the pyrolysis of the remaining oxygen-containing groups and causes the formation of the carbon ring (Dong et al. 2015). All curves confirm the stability of the graphitic structure up to 650 °C. The weight loss of the samples was calculated to be 4%, 6%, 7.3%, 7.6%, and 8.94%, respectively for, PETZ 0.1, PETZ 0.5, PETZ 0.75, PETZ 1.0, and PET 700 respectively revealing that

the produced carbon-based materials. ZnO particles were also seen decorated on these sheets as highlighted by arrows in each case. The dimension of the particles was found safely

Fig. 7 N₂ adsorption–desorption isotherm of plastic bottles after pyrolysis at 700 °C in inert atmosphere in the absence of Zn dust (PET 700) and in the presence of Zn dust of different contents (PETZ 0.1, PETZ 0.5, PETZ 0.75, and PETZ 1.0)



the stability of the samples is in the order: PETZ 0.1 > PETZ 0.5 > PETZ 0.75 > PETZ 1.0 > PET 700.

The N_2 adsorption–desorption measurements of PET 700, PETZ 0.1, PETZ 0.5, PETZ 0.75, and PETZ 1.0 samples are represented in Fig. 7. The adsorption–desorption isotherms of all samples exhibit a mixture of IUPAC type I and type IV. The open loop N_2 adsorption–desorption isotherm is well-known for porosity with ink-bottle-shaped pores and narrow slit pores since the diffusion is very slow inside the pores (Fu et al. 2017). A high adsorption of N_2 (over 90%) under relatively low pressure (0.14) has been observed indicating the presence of mesopores with large pore size distribution, and all values are collected in Table 1. The produced carbon materials presented very high surface area (up to 684.5 m^2/g) with mesopore size distribution (18.47–16.88 nm). The BET surface area and average pore volume decrease with the increase of the ZnO content in the samples which may be attributed to occupying of ZnO on some active sites of the graphite.

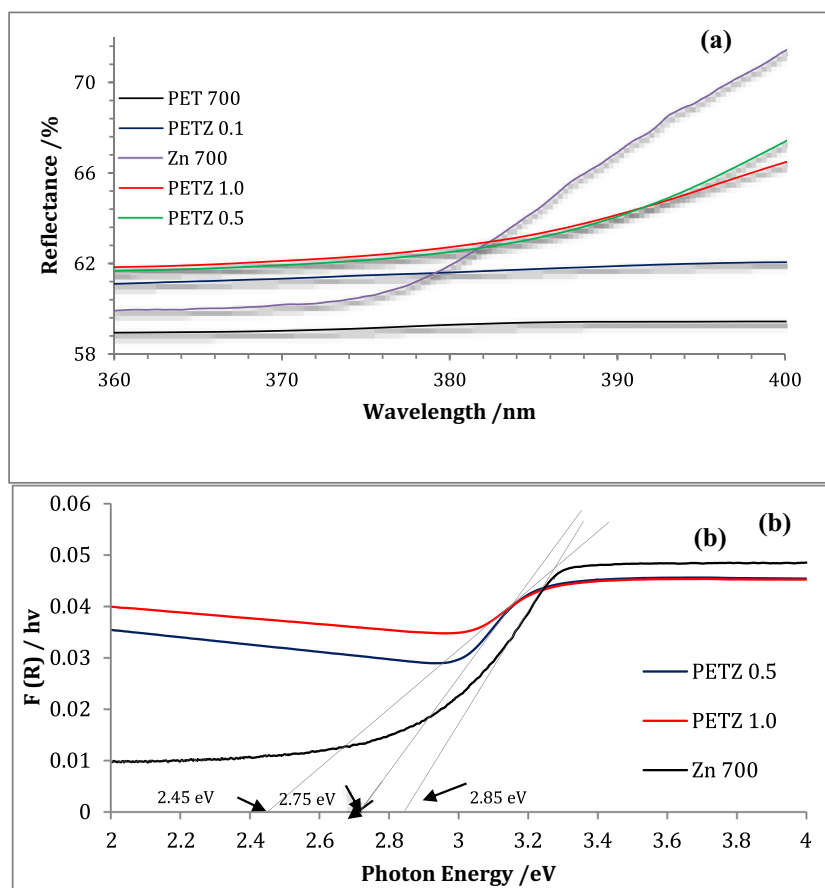
The UV-vis diffuse reflectance spectra of the samples are shown in Fig. 8(a). The reflectance spectra of Zn 700

exhibit the typical UV absorption of ZnO nanoparticles with broad reflection in the visible region of the spectrum. The reflectance value is very much lower for ZnO@Graphite samples, indicating high absorption of light and evidencing that graphite with ZnO extends the absorbance into visible region (380–800 nm). The band gap energy of the all samples was estimated from the plot of transformed Kubelka–Munk function (Fig. 8(b)) to be 2.85 eV and 2.75 eV and 2.5 eV, respectively, for Zn 700 and PETZ 0.5 and PETZ 1.0 respectively evidencing the role of graphite in extending the light absorption to visible range.

Mechanism of simultaneous transformation of Zn/PET mixed waste to ZnO@ porous graphite nanocomposite

Based on the above results, Zn could be completely transformed to ZnO in the presence of PET. It has been reported previously that the pyrolysis of PET produces primarily cyclic oligomers by intermolecular exchange. These oligomers can be further decomposed to form carboxylic acid

Fig. 8 (a) UV-vis diffuse reflectance spectra of plastic bottles after pyrolysis at 700 °C in inert atmosphere in the absence of Zn dust (PET 700) and in the presence of Zn dust of different contents (PETZ 0.1, PETZ 0.5, and PETZ 1.0). (b) The plot of transformed Kubelka–Munk function versus the energy of light



such as terephthalic acid (TPA) and 2,6-naphthalene dicarboxylic acid (NDC) by β -hydrogen transfer (Goodman and Nesbitt 1960; Samperi et al. 2004; Hujuri et al. 2013). TPA and NDC can be reacted with Zn metal at elevated temperature to produce zinc terephthalate and zinc naphthalenedicarboxylate, which were then thermally decomposed to form ZnO and aromatic hydrocarbon. The thermal decomposition of aromatic hydrocarbons can finally lead to the formation of graphite deposits. The mechanism of the simultaneous transformation of plastic bottles and Zn dust into ZnO@Graphite nanocomposite can be proposed as follows:

Photocatalytic performance

The photocatalytic activity of prepared samples has been evaluated by following the degradation of MB and MG dyes as model pollutants under UV light irradiation. Figures 9(a) and 10(a) show the UV-Vis absorption spectra of an aqueous MB and MG dye solution respectively obtained during the photocatalytic degradation over PET 700, PETZ 0.1, PETZ 0.5, PETZ 0.75, and PETZ 1.0 under UV light irradiation. It is obvious that the absorption peak at 665 nm for MB diminishes gradually with irradiation time and completely disappeared after 60 min (see Fig. 9(a)).

Fig. 9 (a) UV-vis absorption spectra of an aqueous solution of MB during illumination in the presence of PETZ 0.1 at pH 6.7. (b) Photocatalytic degradation efficiency of MB as the variation of C/C_0 with irradiation time in the presence of PET 700, PETZ 0.1, PETZ 0.5, PETZ 0.75, and PETZ 1.0

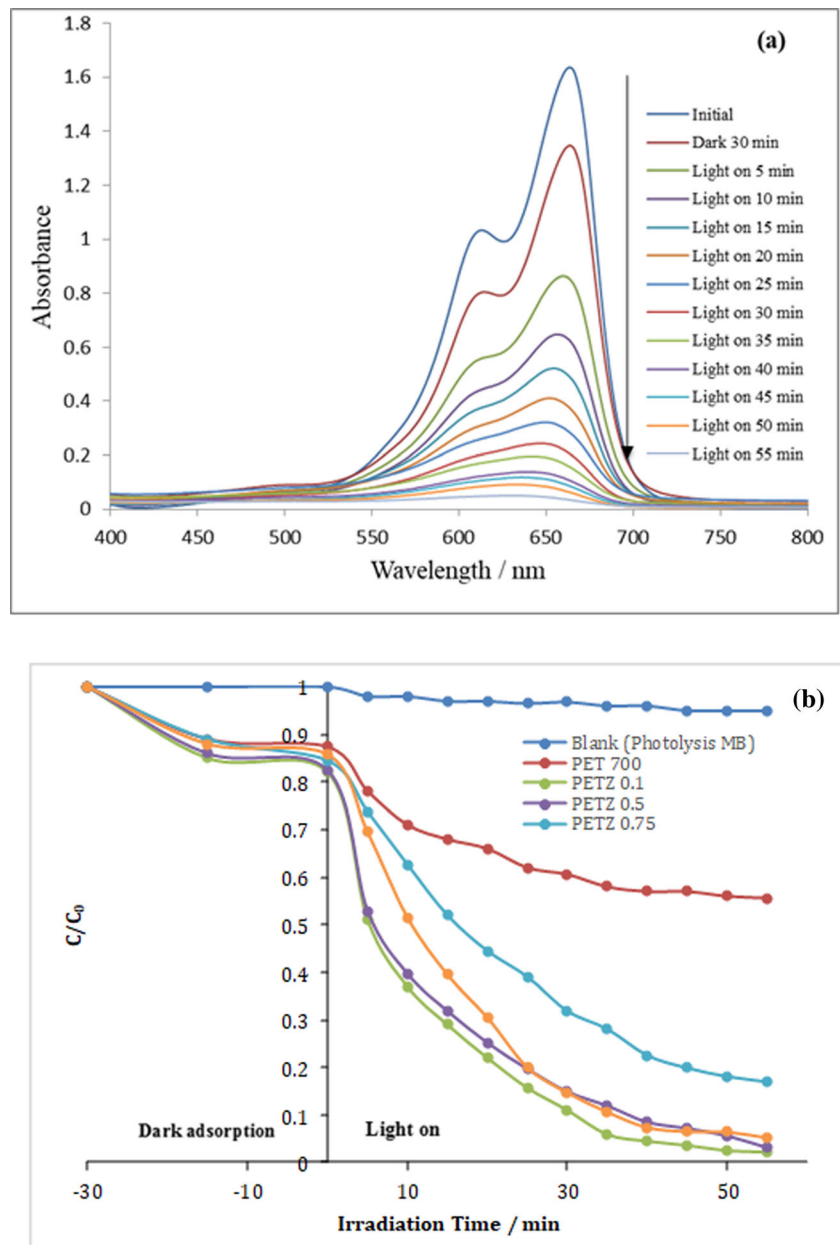
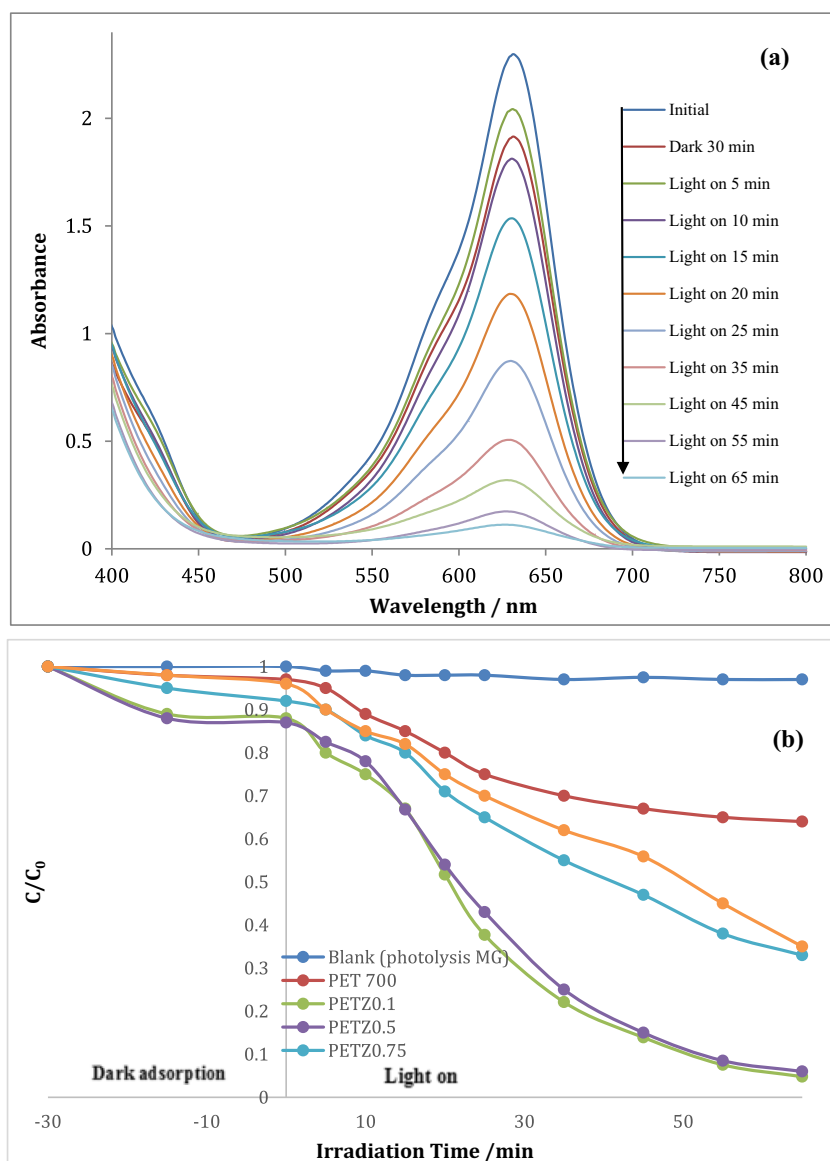


Fig. 10 (a) UV-vis absorption spectra of an aqueous solution of MG during illumination in the presence of PETZ 0.1 at pH 6.7. (b) Photocatalytic degradation efficiency of MG as the variation of C/C° with irradiation time in the presence of PET 700, PETZ 0.1, PETZ 0.5, PETZ 0.75, and PETZ 1.0

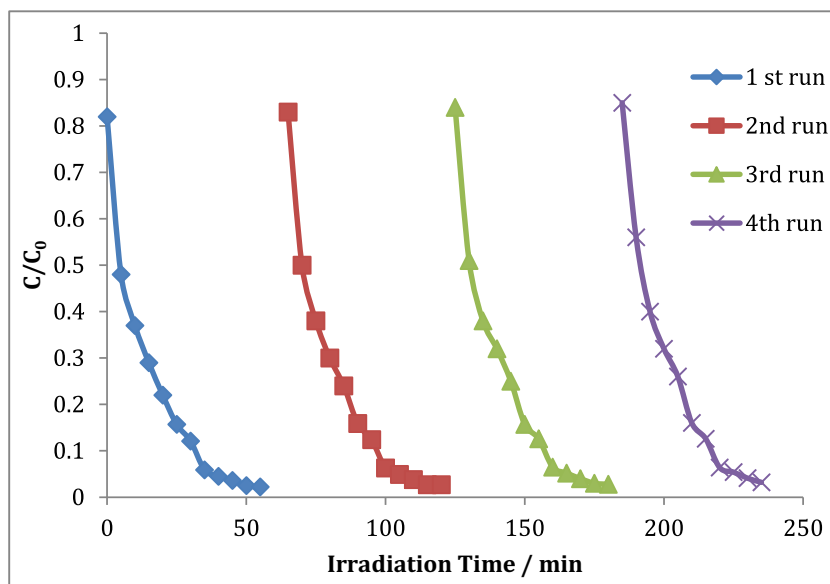


Similarly, the absorption peak at 635 nm for MG dye completely disappears within 70 min (see Fig. 10(a)). Obvious enhancement of the photocatalytic activity of ZnO@Graphite composites (PET 0.1, PET 0.5, PET 0.75, and PET 1.0) can be attributed to the high electron pair separation achieved by the electronic interaction between ZnO and graphite and due to extensive π - π conjugation system (Zhang et al. 2009; Yatskiv and Grym 2018). Figures 9(b) and 10(b) show the degradation efficiency of MB and MG respectively as the variation of C/C° with irradiation time in the presence of PET 700, PETZ 0.1, PETZ 0.5, PETZ 0.75, and PETZ 1.0. It is also obvious that PETZ 0.1 exhibits the highest photocatalytic activity amongst the other samples. At lower Zn concentration (i.e., PETZ 0.1), the produced ZnO particles have narrower particle distribution with higher surface area. Our explanation

is confirmed by the TEM results as well as the BET surface area measurements.

It is very important to evaluate the recyclability of PETZ 0.1 nanocomposite from the environmental application point of view. The recyclability has been evaluated by carrying out the photocatalytic experiment four times using the same nanocomposite. After each run, the nanocomposite particles were collected and then washed by distilled water three times by centrifugation and then dried at 60 for 1 h for the use in the next run. Figure 11 shows the results of the recycle use of PET 0.1 (1 g/l) for the degradation of MB (20 ppm), at pH 6.7. It is obvious that there is almost no change in the photocatalytic efficiency of the nanocomposite after the four-recycle use evidencing the excellent stability of the nanocomposite-based waste.

Fig. 11 Recycle use of PET 0.1 (1 g/l) for the photocatalytic degradation of MB (20 ppm), at pH 6.7



Conclusions

Mesoporous ZnO/graphite nanocomposites have been successfully created from Zn dust/PET bottle mixed waste utilizing facile pyrolysis method. The crystal structure, morphology, and surface area of produced materials were investigated using different techniques. It was found that, while no transformation of Zn metal to ZnO nanoparticles in the absence of PET bottle waste is observed, simultaneous transformation of Zn into ZnO and transformation of the bottle waste into mesoporous graphite have been occurred upon thermal treatment at 700 °C in inert atmosphere. The mixed waste-based nanocomposites exhibited a superior photocatalytic activity for the degradation of organic dyes (methylene blue and malachite green) under UV irradiation. It was shown that the dyes have been completely degraded after 60–70 min. Obvious enhancement of the photocatalytic activity of ZnO@Graphite composites (PET 0.1, PET 0.5, PET 0.75, and PET 1.0) can be attributed to the high electron pair separation achieved by the electronic interaction between ZnO and graphite and due to extensive π - π conjugation system. Since plastic and metal waste can exist together in several manufactures such as electronic waste, medical waste, batteries, accumulators, and end-of-life vehicles, upcycling plastic/metal mixed waste is considered to be a mature field of interest owing to its perilous impact on human life and environment. The presented method can be applied to different metal/plastic mixed waste systems, and the produced nanocomposite materials can be applied in various photocatalytic systems. This work is believed to be an innovative and sustainable approach of creating active nanomaterials as utilizing hazardous and waste materials and minimal costs simple technique as well as introducing a new way of upcycling mixed waste materials.

Acknowledgements The authors gratefully acknowledge the research units at College of Science and Institute for Research and Medical Consultations, Imam Abdulrahman Bin Faisal University.

Funding information This work is financially supported by the Deanship of Scientific Research of Imam Abdulrahman Bin Faisal University, Saudi Arabia (Grant Nos. 2016-074-Sci).

Publisher's note Springer Nature remains neutral with regard to jurisdictional claims in published maps and institutional affiliations.

References

- Ajji A et al (1995) Amorphous orientation of poly (ethylene terephthalate) by X-ray diffraction in combination with Fourier transform infra-red spectroscopy. *Polymer Elsevier* 36(21):4023–4030
- Akhavan O, Bijanzadm K, Mirsepah A (2014) Synthesis of graphene from natural and industrial carbonaceous wastes. *RSC Adv* 4: 20441–20448
- Anene AF et al (2018) Experimental study of thermal and catalytic pyrolysis of plastic waste components. *Sustainability* 10:3979
- Buekens AG, Huang H (1998) Catalytic plastics cracking for recovery of gasoline-range hydrocarbons from municipal plastic wastes. *Resour Conserv Recycl Elsevier* 23(3):163–181
- Chen J-C, Tang C-T (2007) Preparation and application of granular ZnO/Al₂O₃ catalyst for the removal of hazardous trichloroethylene. *J Hazard Mater Elsevier* 142(1–2):88–96
- Chen D et al (2015) Reprint of: pyrolysis technologies for municipal solid waste: a review. *Waste Manag Elsevier* 37:116–136
- Dai H (2002) Carbon nanotubes: opportunities and challenges. *Surf Sci Elsevier* 500(1–3):218–241
- De Volder MFL et al (2013) Carbon nanotubes: present and future commercial applications. *Sci Am Assoc Adv Sci* 339(6119):535–539
- Dědková K et al (2015) ZnO/graphite composites and its antibacterial activity at different conditions. *J Photochem Photobiol B* 151:256–263
- Dervishi E et al (2009) Carbon nanotubes: synthesis, properties, and applications. *Part Sci Technol Taylor & Francis* 27(2):107–125

- Ding Y et al (2016) Cellulose tailored Anatase TiO₂ nanospindles in three-dimensional graphene composites for high-performance supercapacitors. *ACS Appl Mater Interfaces* 8(19):12165–12175
- Ding J et al (2017) Hydroxylated graphene-based flexible carbon film with ultrahigh electrical and thermal conductivity. *Nanotechnology* 28:395404
- Dong Y et al (2015) Graphene/acid assisted facile synthesis of structure-tuned Fe₃O₄ and graphene composites as anode materials for lithium ion batteries. *Carbon Elsevier* 86:310–317
- Dvorak P, Jandova J (2005) Hydrometallurgical recovery of zinc from hot dip galvanizing ash. *Hydrometallurgy Elsevier* 77(1–2):29–33
- Esfandiari A, Kaghazchi T, Soleimani M (2012) Preparation and evaluation of activated carbons obtained by physical activation of polyethyleneterephthalate (PET) wastes. *J Taiwan Inst Chem Eng Elsevier* 43(4):631–637
- Fu H et al (2017) Characteristics of pore structure and fractal dimension of low-rank coal: a case study of lower Jurassic Xishanyao coal in the southern Junggar Basin, NW China. *Fuel* 193:254–264
- Geim AK, Novoselov KS (2007) The rise of graphene. *Nat Mater. Nature Publishing Group* 6(3):183
- Goodman I, Nesbitt BF (1960) The structures and reversible polymerization of cyclic oligomers from poly(ethylene terephthalate). *Polymer* 1:384–396
- Gottardi S et al (2014) Self-assembly: cyano-functionalized triarylamines on au(111): competing intermolecular versus molecule/substrate interactions. *Adv Mater Interfaces* 2014(1):1300150
- Gupta A, Johnson EF, Schlossel RH (1987) Investigation into the ion exchange of the cyanide complexes of zinc (2+), cadmium (2+), and copper (1+) ions. *Ind Eng Chem Res. ACS Publications* 26(3):588–594
- Howard JB et al (1991) Fullerenes C₆₀ and C₇₀ in flames. *Nature. Nature Publishing Group* 352(6331):139
- Howard JB, Chowdhury KD, Vander Sande JB (1994) Carbon shells in flames. *Nature. Nature Publishing Group* 370(6491):603
- Hujuri U, Ghoshal AK, Gumma S (2013) Temperature-dependent pyrolytic product evolution profile for polyethylene terephthalate. *J Appl Polym Sci* 130:3993–4000
- Irwin RJ et al (1997) Environmental contaminants encyclopedia: Lead entry. National Parks Service, Water Resources Division, Fort Collins
- Jadhav U, Hocheng H (2015) Hydrometallurgical recovery of metals from large printed circuit board pieces. *Sci Rep Nat Publ Group* 5:14574
- Jan MR, Shah J, Gulab H (2013) Catalytic conversion of waste high-density polyethylene into useful hydrocarbons. *Fuel. Elsevier* 105:595–602
- Kim SC, Kim SJ, Yu EY (1997) The effect of alkali metal salts on ZnO-Al₂O₃ and MnO₂ catalysts for the oxidative coupling of methane. *Appl Catal A Gen. Elsevier* 150(1):63–76
- Lerici LC, Renzini MS, Pierella LB (2015) Chemical catalyzed recycling of polymers: catalytic conversion of PE, PP and PS into fuels and chemicals over HY. *Procedia Mater Sci. Elsevier* 8:297–303
- Leung AOW et al (2008) Heavy metals concentrations of surface dust from e-waste recycling and its human health implications in Southeast China. *Environ Sci Technol ACS Publications* 42(7):2674–2680
- Linden D (1995) Handbook of batteries. In: Fuel and energy abstracts, p 265
- Lin-Vien D et al (1991) The handbook of infrared and Raman characteristic frequencies of organic molecules. Elsevier
- Lovett S, Berruti F, Behie LA (1997) Ultraprolytic upgrading of plastic wastes and plastics/heavy oil mixtures to valuable light gas products. *Ind Eng Chem Res. ACS Publications* 36(11):4436–4444
- Mauter MS, Elimelech M (2008) Environmental applications of carbon-based nanomaterials. *Environ Sci Technol* 42(16):5843–5859
- Memon MA, Bai W, Sun J, Imran M, Phulpoto SN, Yan S, Huang Y, Geng J (2016) Conjunction of conducting polymer nanostructures with macroporous structured graphene thin films for high-performance flexible supercapacitors. *ACS Appl Mater Interfaces* 8(18):11711–11719
- Mhamane D et al (2011) From graphite oxide to highly water dispersible functionalized graphene by single step plant extract-induced deoxygenation. *Green Chem R Soc Chem* 13(8):1990–1996
- Mishra N et al (2012) Pyrolysis of waste polypropylene for the synthesis of carbon nanotubes. *J Anal Appl Pyrolysis. Elsevier* 94:91–98
- Miskolczi N et al (2009) Fuels by pyrolysis of waste plastics from agricultural and packaging sectors in a pilot scale reactor. *Fuel Process Technol Elsevier* 90(7–8):1032–1040
- Mohamed HH (2018) Sonochemical synthesis of ZnO hollow microstructure/reduced graphene oxide for enhanced sunlight photocatalytic degradation of organic pollutants. *J Photochem Photobiol A Chem* 353:401–408
- Mohamed HH, Alsanea A (2018) TiO₂/carbon dots decorated reduced graphene oxide composites from waste car bumper and TiO₂ nanoparticles for photocatalytic applications. *Arab J Chem, In press. <https://doi.org/10.1016/j.arabjc.2018.08.016>*
- Mohamed HH, Mohamed SK (2018) Rutile TiO₂ nanorods/MWCNT composites for enhanced simultaneous photocatalytic oxidation of organic dyes and reduction of metal ions. *Mater Res Express* 5:015057
- Mohamed et al (2018) Multifunctional TiO₂ microspheres-rGO as highly active visible light photocatalyst and antimicrobial agent. *Mater Express* 8(4):345–352
- Morf LS et al (2013) Precious metals and rare earth elements in municipal solid waste—sources and fate in a Swiss incineration plant. *Waste Manag Elsevier* 33(3):634–644
- Murthy NS, Correale ST, Minor H (1991) Structure of the amorphous phase in crystallizable polymers: poly (ethylene terephthalate). *Macromolecules ACS Publications* 24(5):1185–1189
- Muthirulan PM et al (2013) Beneficial role of ZnO photocatalyst supported with porous activated carbon for the mineralization of alizarin cyanin green dye in aqueous solution. *J Adv Res* 6:479–484
- Nasir S, Hussein M, Zainal Z, Yusof N (2018) Carbon-based nanomaterials/allotropes: a glimpse of their synthesis, properties and some applications. *Materials* 11:295. <https://doi.org/10.3390/ma11020295>
- Paquin R, Limage M-H, Colombar P (2007) Micro-Raman study of PET single fibres under high hydrostatic pressure: phase/conformation transition and amorphization. *J Raman Spectrosc Wiley Online Library* 38(9):1097–1105
- Popov VN (2004) Carbon nanotubes: properties and application. *Mater Sci Eng R Rep Elsevier* 43(3):61–102
- Richter H et al (1997) Generation of higher fullerenes in flames. *J Phys Chem B ACS Publications* 101(9):1556–1560
- Ruan G, Sun Z, Peng Z, Tour JM (2011) Growth of graphene from food, insects, and waste. *ACS Nano* 5(9):7601–7607
- Samperi F, Puglisi C, Alicata R, Montaudo G (2004) Thermal degradation of poly(butylene terephthalate) at the processing temperature. *Polym Degrad Stab* 83:11–17
- Schmucker SC (1893) The electrolytic separation of the metals of the second group. *J Am Chem Soc ACS Publications* 15(4):195–206
- Sharma BK et al (2014) Production, characterization and fuel properties of alternative diesel fuel from pyrolysis of waste plastic grocery bags. *Fuel Process Technol Elsevier* 122:79–90
- Shinde VV et al (2014) Surfactant free microwave assisted synthesis of ZnO microspheres: study of their antibacterial activity. *Appl Surf Sci Elsevier* 307:495–502
- Singh et al (2016) Graphene oxide: strategies for synthesis, reduction and frontier applications. *RSC Adv* 6:64993–65011
- Socrates G (2001) Infrared and Raman characteristic group frequencies: tables and charts. John Wiley & Sons

- Tang T et al (2005) Synthesis of multiwalled carbon nanotubes by catalytic combustion of polypropylene. *Angewandte Chemie International Edition Wiley Online Library* 44(10):1517–1520
- To JWF et al (2015) Ultrahigh surface area three-dimensional porous graphitic carbon from conjugated polymeric molecular framework. *ACS Cent Sci* 1:68–76
- Vander Hoogerstraete T, Onghena B, Binnemans K (2013) Homogeneous liquid–liquid extraction of metal ions with a functionalized ionic liquid. *J Phys Chem Lett. ACS Publications* 4(10):1659–1663
- Xu J, Wang Y, Hu S (2017) Nanocomposites of graphene and graphene oxides: synthesis, molecular functionalization and application in electrochemical sensors and biosensors. A review. *Microchim Acta* 184:1–44
- Yang M-H, Lin Y-H (2009) Catalytic conversion of postconsumer PE/PP waste into hydrocarbons using the FCC process with an equilibrium FCC commercial catalyst. *J Appl Polym Sci Wiley Online Library* 114(1):193–203
- Yatskiv R, Grym J (2018) Influence of the interaction between graphite and polar surfaces of ZnO on the formation of Schottky contact. *J Electron Mater* 47:5002–5006
- Zhang L, Cheng H, Zong R, Zhu Y (2009) Photocorrosion suppression of ZnO nanoparticles via hybridization with graphite-like carbon and enhanced photocatalytic activity. *J Phys Chem C* 113(6):2368–2374
- Zhao YL et al (2017) ZnO Nanomembrane/expanded graphite composite synthesized by atomic layer deposition as binder-free anode for Lithium ion batteries. *ACS Appl Mater Interfaces* 9:38522–38529
- Zhou Y, Qiu K (2010) A new technology for recycling materials from waste printed circuit boards. *J Hazard Mater Elsevier* 175(1–3):823–828
- Zhou H, Liu Q, Liu W, Ge J, Lan M, Wang C, Geng J, Wang P (2014) Template-free preparation of Volvox-like Cd_xZn_{1-x}S Nanospheres with cubic phase for efficient photocatalytic hydrogen production. *Chem-Asian J* 9:811–818
- Zhuo C, Levendis YA (2014) Upcycling waste plastics into carbon nanomaterials: a review. *J Appl Polym Sci Wiley Online Library* 131(4)